
Reviving Stale Updates: Data-Free Knowledge Distillation for Asynchronous Federated Learning

Baris Askin^{1†} Holger R. Roth² Zhenyu Sun^{3†} Carlee Joe-Wong¹ Gauri Joshi¹ Ziyue Xu²

Abstract

Federated learning (FL) enables collaborative model training across distributed clients without sharing raw data, yet its scalability is limited by synchronization overhead. Asynchronous federated learning (AFL) alleviates this issue by allowing clients to communicate independently, thereby improving wall-clock efficiency in large-scale, hardware-heterogeneous environments. However, asynchrony introduces updates computed on outdated global models (*staleness*) that can destabilize optimization and hinder convergence. We propose FedRevive, an AFL framework that revives stale updates through data-free knowledge distillation (DFKD). FedRevive integrates parameter-space aggregation with a lightweight, server-side DFKD process that transfers knowledge from stale client updates to the current global model without access to data. A meta-learned generator synthesizes pseudo-samples used for multi-teacher distillation. A hybrid aggregation scheme that combines raw with DFKD updates effectively mitigates staleness while retaining AFL scalability. Experiments on various vision and text benchmarks show that FedRevive achieves faster training by up to 38.4% and higher final accuracy by up to 16.5% than asynchronous baselines.

1. Introduction

Modern artificial intelligence models thrive on large amounts of data, which raises serious concerns about privacy and regulatory compliance (Yang et al., 2019). Federated learning (FL) addresses this dilemma by enabling many clients (e.g., smartphones, wearables, hospital servers) to collaboratively train a shared model without uploading raw data (McMahan et al., 2017). In vanilla FL, the server broadcasts the current global model, clients perform local training

on private data, and the server aggregates returned updates to form the next global iterate. This paradigm preserves data locality and widens access to otherwise restricted data, while reducing central storage risks. Moreover, relying only on public datasets is increasingly insufficient, as large models saturate public corpora and demand broader coverage across domains. FL supports both cross-silo (e.g., hospitals and enterprises) and cross-device (e.g., millions of phones) settings, offering a practical path to leverage diverse private data at scale (Rieke et al., 2020; Lai et al., 2021).

In *synchronous* FL, the server waits for all (or a selected subset of) participating clients to complete their local updates before aggregation (McMahan et al., 2017). Although this strategy aligns updates to the same global state, it suffers from the *straggler problem*: slow or unavailable clients delay the entire round, leading to underutilized resources and poor scalability under heterogeneous availability and compute capacity (Xie et al., 2019). *Asynchronous* FL (AFL) alleviates this bottleneck by allowing the server to incorporate each client update upon arrival, without waiting for others (Xie et al., 2019; Nguyen et al., 2022). Clients train and communicate independently, and the server continuously updates the global model. This design improves wall-clock efficiency and makes AFL appealing for cross-device deployments such as mobile networks and for cross-silo collaborations where institutional availability fluctuates.

The flexibility of AFL, however, comes with a major drawback: *update staleness*. Since clients may train on older global checkpoints, the server receives delayed updates that no longer match the current optimization state, which can distort training dynamics and degrade performance, especially under not independently and identically distributed (non-IID) data (Xie et al., 2019; Nguyen et al., 2022; Askin et al., 2024; Richtarik, 2025). This issue becomes more pronounced as the system scales, since larger deployments naturally exhibit a wider spread of client runtimes and delays (Koloskova et al., 2022). Existing AFL methods mitigate staleness by buffering or smoothing arriving updates (Nguyen et al., 2022) or by explicitly correcting or down-weighting delayed updates (Chen et al., 2021). While effective in certain regimes, these strategies can slow server progress or suppress information carried by slower clients.

[†]Work was done during an internship at NVIDIA. ¹Carnegie Mellon University ²NVIDIA ³Northwestern University. Correspondence to: Baris Askin <baskin@andrew.cmu.edu>.

Even a delayed update can encode rich signals about a client’s local data. The key challenge is therefore not only to control the harmful drift induced by staleness, but also to retain the useful knowledge in delayed client models. This motivates the following question:

*Can we **revive** stale updates in asynchronous FL to extract useful knowledge for improved scalability?*

Our idea: distill knowledge from stale updates. We answer this question by combining parameter-space aggregation with *data-free knowledge distillation* (DFKD). Knowledge distillation (KD) transfers information from one or more teachers to a student via softened targets or intermediate representations (Hinton et al., 2015). Data-free variants remove the assumption that a public dataset is available for distillation (Lopes et al., 2017), which aligns with practical FL deployments. At a high level, our method treats received client models as teachers and the current server model as the student, and uses server-side DFKD to extract transferable knowledge from delayed client states. Then, by coupling regular parameter space update with a DFKD update, our method mitigates the adverse effects of staleness. Integrating DFKD into AFL is nontrivial because (i) no data are typically available in the server, (ii) stale client models can be heterogeneous and usually have poor performance, and (iii) the distillation step must remain lightweight to preserve AFL’s scalability advantages. Our design addresses these issues and extracts information from delayed updates in a data-free manner, improving training speed and accuracy.

Related work. AFL has been explored as a practical remedy for stragglers by integrating updates upon arrival rather than at synchronized rounds (Xie et al., 2019; Nguyen et al., 2022; Xu et al., 2023; Chen et al., 2020; Richtarik, 2025). To mitigate staleness, prior work explores buffering or delay-aware reweighting strategies that control instability but can also attenuate information from slower clients (Nguyen et al., 2022; Chen et al., 2019; Shi et al., 2020; Lu et al., 2020; Zhang et al., 2016; Dutta et al., 2018; Cui et al., 2014). In parallel, knowledge distillation (KD) is tool for transferring predictive structure from teachers to students (Hinton et al., 2015), and has been adapted to FL to mitigate heterogeneity, support model-architecture mismatch, and improve privacy via logits or ensemble-based supervision (Li & Wang, 2019; Lin et al., 2020; Qin et al., 2024; Fan et al., 2024). These FL-KD methods typically assume access to a shared dataset for distillation, either on the server or on clients (Lee et al., 2020; Itahara et al., 2021). DFKD removes this dependency by synthesizing pseudo-samples for distillation without real data (Lopes et al., 2017; Mansourian et al., 2025; Fang et al., 2022), and several recent works adopt DFKD within synchronous FL to avoid public data while improving robustness under non-IID data (Gao et al.,

2025; Zhang et al., 2022; Zhu et al., 2021b). However, the use of KD in asynchronous FL remains largely unexplored. Some efforts rely on public data assumptions often unrealistic in FL deployments (Lu et al., 2025). Unlike synchronous FL, where distillation leverages relatively stable teacher models, AFL distills from client models misaligned with the current server state. This makes it nontrivial to design a data-free distillation mechanism for delayed arrivals of highly biased teachers. Appendix A presents an extended related work discussion.

Contributions. The main contributions of the paper are summarized as follows:

- We propose FedRevive, an AFL framework that *revives* stale client updates by combining parameter aggregation with server-side, multi-teacher DFKD.
- We carefully design a DFKD pipeline tailored to AFL without requiring any extra client metadata beyond regular FL updates. We leverage a multi-teacher distillation with computation-light process to operationalize our idea.
- We demonstrate improved speed and accuracy over the baseline methods under realistic simulations with image and text-domain experiments, achieving faster time-to-target accuracy and better final performance, and support the proposed method with ablation studies.

Our results indicate that stale client updates still carry rich, transferable knowledge. By extracting that knowledge in a data-free manner and fusing it with parameter-space aggregation, AFL can retain its scalability advantages without sacrificing model quality.

2. FL Problem & Proposed Method

Problem formulation. We consider an FL setup with N clients collaboratively training a global model $\mathbf{x} \in \mathbb{R}^d$. Each client i has a local objective function $f_i : \mathbb{R}^d \rightarrow \mathbb{R}$, defined on private data. Local objectives are different across clients due to heterogeneity in data distribution. The goal of FL is to find \mathbf{x} minimizing the global objective, formulated as the average of local losses, $\frac{1}{N} \sum_{i \in [N]} f_i(\mathbf{x})$.

Asynchronous framework. We first describe a generic AFL framework that encompasses both existing asynchronous schemes (Xie et al., 2019; Nguyen et al., 2022) and our proposed method, FedRevive. The overall process is summarized in Algorithm 1. After model initialization (line 2), the server sends $\mathbf{x}^{(0)}$ to N_a randomly selected active clients for local training. Then, for each server step t , the server waits for the next returned model $\tilde{\mathbf{x}}_i^{(t-\tau_i^t)}$ from some client i (line 4), where τ_i^t denotes the staleness, namely, how many server updates occurred since the client is requested local training. The server processes the client update via an aggregation rule (line 6), and dispatches the updated model

Algorithm 1 Generic AFL Framework

Server Process:

- 1: **Inputs:** Initial model $\mathbf{x}^{(0)}$, server and client learning rates η_s and η_c , #local iterations K , #rounds T , #selected active clients N_a .
- 2: Send $\mathbf{x}^{(0)}$ to N_a randomly selected active clients.
- 3: **for** $t = 0$ **to** $T - 1$ **do**
- 4: **Wait** until the server receives an τ_i^t -stale updated model $\tilde{\mathbf{x}}_i^{(t-\tau_i^t)}$ from client i .
- 5: Client update $\Delta_i^{(t-\tau_i^t)} \leftarrow \tilde{\mathbf{x}}_i^{(t-\tau_i^t)} - \mathbf{x}^{(t-\tau_i^t)}$.
- 6: **Process update using one of Eq.s (1), (2), or (3).**
- 7: Assign local training to a randomly selected active client with the updated model $\mathbf{x}^{(t+1)}$.
- 8: **end for**

Client i 's Local Training (Async. and Parallel):

- 9: **Input:** Received server model \mathbf{x} .
- 10: Initialize $\tilde{\mathbf{x}} \leftarrow \mathbf{x}$.
- 11: **for** $k = 1$ **to** K **do**
- 12: $\tilde{\mathbf{x}} \leftarrow \tilde{\mathbf{x}} - \eta_c \tilde{\nabla} f_i(\tilde{\mathbf{x}})$ {A stoch. grad. update}
- 13: **end for**
- 14: **Return** $\tilde{\mathbf{x}}$ to the server.

$\mathbf{x}^{(t+1)}$ to a randomly selected active client (line 7) to sustain parallelism. Different AFL variants share this control flow and differ only in the aggregation step, that is, how the server maps $(\mathbf{x}^{(t)}, \Delta_i^{(t-\tau_i^t)})$ to $\mathbf{x}^{(t+1)}$.

Vanilla and buffered AFL. Vanilla AFL algorithm (Xie et al., 2019) updates the global model immediately when a client update arrives. Accordingly, the aggregation step in Algorithm 1 (line 6) becomes:

$$\mathbf{x}^{(t+1)} \leftarrow \mathbf{x}^{(t)} + \eta_s \Delta_i^{(t-\tau_i^t)} \quad (1)$$

While this rule is simple and maximally asynchronous, it makes staleness accumulate fast. Every time the server updates \mathbf{x} , all clients that are still training are effectively one step further behind. When staleness, τ_i^t is large, the returned update can yield a biased step and lead to oscillations or divergence. FedBuff (Nguyen et al., 2022) mitigates this by buffering updates before applying them. The server maintains a buffer \mathcal{B} of size B , stores incoming client updates, and aggregates only when B updates have been collected. The aggregation step in Algorithm 1 (line 6) becomes:

$$\begin{aligned} &\mathcal{B} \leftarrow \mathcal{B} \cup \{\Delta_i^{(t-\tau_i^t)}\} \\ \text{if } |\mathcal{B}| = B : &\mathbf{x}^{(t+1)} \leftarrow \mathbf{x}^{(t)} + \frac{\eta_s}{B} \sum_{\Delta \in \mathcal{B}} \Delta \quad \text{and } \mathcal{B} \leftarrow \emptyset \\ \text{else: } &\mathbf{x}^{(t+1)} \leftarrow \mathbf{x}^{(t)} \end{aligned} \quad (2)$$

The buffered strategy smooths the staleness effect by reducing the update frequency. Yet, as the buffer size B increases, the infrequent server updates slow down the training. Next, we describe our method, FedRevive, mitigating the staleness

without reducing the server model update frequency.

2.1. Overview of FedRevive

FedRevive addresses the staleness problem by leveraging knowledge-distillation. Although directly aggregating the parameters of stale updates can result in training instabilities, received update still contains informative signals shaped by the client data. Our approach augments the standard parameter-space update with a data-free knowledge distillation (DFKD) signal extracted from the updated client model.

FedRevive aggregation. In FedRevive, the server adaptively fuses the conventional parameter-space update with a knowledge-distilled update to alleviate the adverse effect of staleness. When the server receives a τ_i^t -stale client update $\Delta_i^{(t-\tau_i^t)}$, it first obtains a knowledge-distilled update through a DFKD process. The server then combines it with original parameter update through an adaptive weighting function $\beta(\tau_i^t) \in [0, 1]$ controlling the reliance on the knowledge-distilled signal according to the degree of staleness. The aggregation step in Algorithm 1 (line 6) becomes:

$$\begin{aligned} \Delta_i^{\text{KD}} &\leftarrow \text{KD-Revive}(\tilde{\mathbf{x}}_i^{(t-\tau_i^t)}, \mathbf{x}^{(t)}), \\ \mathbf{x}^{(t+1)} &\leftarrow \mathbf{x}^{(t)} + \eta_s [(1 - \beta(\tau_i^t)) \Delta_i^{(t-\tau_i^t)} + \beta(\tau_i^t) \Delta_i^{\text{KD}}] \end{aligned} \quad (3)$$

where $\text{KD-Revive}(\cdot)$ encapsulates our proposed DFKD mechanism. The function $\beta : \mathbb{N}_0 \rightarrow [0, 1]$ is a non-decreasing mapping of the staleness τ_i^t , such that the server increasingly relies on the KD-based update as the client update becomes more outdated. Intuitively, when $\tau_i^t \approx 0$, the client model is nearly up-to-date, and the raw parameter update remains reliable, so $\beta(\tau_i^t) \approx 0$; conversely, when τ_i^t is large, $\beta(\tau_i^t) \approx 1$, distilled knowledge extracted from the stale client model is weighted more. The choice of $\beta(\tau_i^t)$ is detailed in Section 3.

Challenges of integrating KD in AFL. Integrating KD into AFL is complicated by the absence of shared data at the server, continually changing teacher models, and client heterogeneity. We first provide an overview of the main issues and how FedRevive addresses them.

(a) *Lack of distillation data.* Standard KD practice requires data to mediate the knowledge transfer between the teacher and the student models. In FL, a public or server-accessible dataset is rarely available due to privacy and communication constraints. Our KD-Revive module performs data-free KD and synthesizes pseudo-inputs guided jointly by the incoming client model and the current server model, enabling distillation without access to real data. Note that FedRevive only uses standard federated updates as in FedAvg (McMahan et al., 2017). Generated pseudo-samples do not provide extra information and are simply intermediate computations for extracting knowledge from already-received updates.

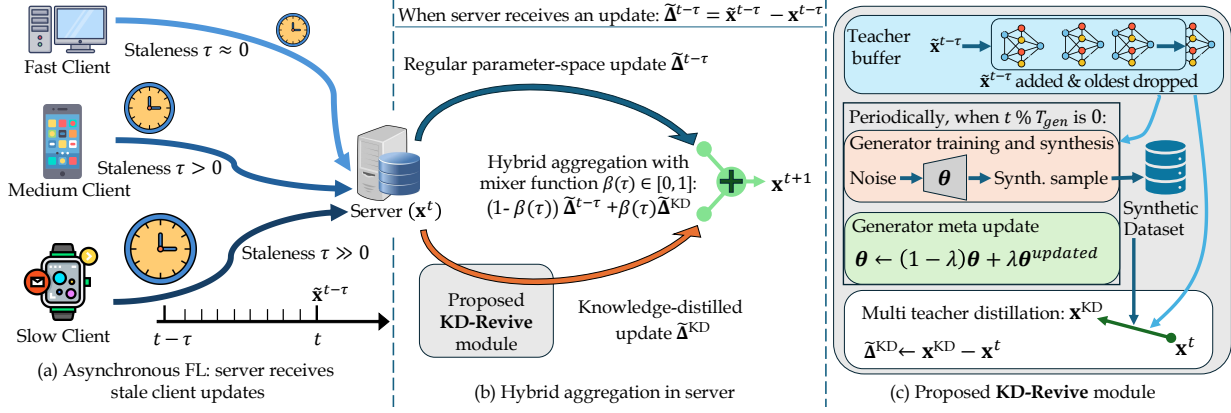


Figure 1. Proposed FedRevive framework.

(b) *Dynamic teachers and need for lightweight operations.* Teacher models in KD or DFKD setups are typically frozen and fully trained oracles. In FL, however, client models continually evolve and are only partially trained. Transferring knowledge from such transient teachers is non-trivial. Moreover, the overhead due to the distillation process must remain computationally light to avoid a new bottleneck. We adopt a lightweight meta-learning strategy inspired by Fang et al. (2022), maintaining a single generator that evolves throughout training. This generator efficiently adapts at every T_{gen} round to the incoming client models and synthesizes pseudo-samples to extend the synthetic KD dataset (\mathcal{D}_{KD}), initialized empty in the beginning of the training.

(c) *Data heterogeneity across clients.* Due to limited data size and non-IID distributions, each client’s update tends to overfit to its local data, which leads to biased knowledge transfer. We mitigate this via *multi-teacher distillation*. The server maintains a buffer \mathcal{C} of the most recent received c client models and distills from all buffered teachers jointly. To better exploit client-specific information, the server derives proxy class proportions of clients from the received updates *without additional information*. Our results do not assume access to extra information beyond regular updates.

Per-client class-proportion proxies from regular updates.

To weight buffered teachers in a class-aware manner, we associate each client i with a *proxy* class-proportion vector $\hat{\pi}_i \in \mathcal{S}^C$ where C denotes the number of classes, \mathcal{S}^C denotes C -simplex, and $\hat{\pi}_i^j = [\hat{\pi}_i]_j$ denotes the proxy proportion of class j on client i . The server computes $\hat{\pi}_i$ using only the regular updates and server-side forward passes, requiring *no additional client computation or information*.

Let $\mathbf{y}_i^{(u)}$ denote the u -th model upload received from client i (ordered by server reception), and consider the first T_{est} uploads $\{\mathbf{y}_i^{(u)}\}_{u=1}^{T_{\text{est}}}$. For each upload, the server probes $\mathbf{y}_i^{(u)}$ with a batch of random inputs \mathbf{r} (Gaussian noise for vision models, random token sequences for language models), and

computes a per-upload proxy:

$$\tilde{\pi}_i^{(u)} = (1/|\mathbf{r}|) \sum_{r \in \mathbf{r}} \sigma(\mathbf{y}_i^{(u)}(r)), \quad u = 1, \dots, T_{\text{est}},$$

where σ denotes softmax function. The server then averages these vectors and keeps this proxy fixed for the remainder of training, $\hat{\pi}_i \leftarrow \frac{1}{T_{\text{est}}} \sum_{u=1}^{T_{\text{est}}} \tilde{\pi}_i^{(u)}$, and uses running-average for $u < T_{\text{est}}$. This adds negligible server overhead since it only requires forward passes and T_{est} is small (2 in our experiments), while imposing no additional client-side computation. Although this proxy is noisy, FedRevive is empirically robust to its errors. We provide additional details and experiments in Appendix B.

2.2. Detailed Steps of KD-Revive

When the server receives an updated model $\tilde{\mathbf{x}}_i^{(t-\tau_i^t)}$ from client i (Algorithm 1, line 4), it executes KD-Revive to compute a data-free knowledge-distilled update (Eq. 3). This procedure consists of four steps: (i) updating the model buffer, (ii) periodic generator training and sample synthesis, (iii) meta-update of the generator, and (iv) multi-teacher distillation. FedRevive framework is depicted in Figure 1.

(1) Update the model buffer. The server maintains a KD buffer \mathcal{C} storing c most recently received client models to use as teachers. Receiving $\tilde{\mathbf{x}}_i^{(t-\tau_i^t)}$, the buffer is updated as:

$$\mathcal{C} \leftarrow \mathcal{C} \cup \{\tilde{\mathbf{x}}_i^{(t-\tau_i^t)}\} \setminus \{\text{oldest model in } \mathcal{C}\}.$$

The rolling buffer ensures that the distillation process utilizes recent and diverse client knowledge. Let \mathcal{I}_t denote the set of client indices whose models are currently buffered. For class-aware weighting, we normalize the proxy client proportions across buffered teachers, for each class j and client $i \in \mathcal{I}_t$: $\hat{\omega}_i^j \triangleq \hat{\pi}_i^j / \sum_{k \in \mathcal{I}_t} \hat{\pi}_k^j$ so that $\sum_{i \in \mathcal{I}_t} \hat{\omega}_i^j = 1$ for every class j . We use $\hat{\omega}_i^j$ to weight teacher contributions in subsequent steps.

(2) Periodic generator training and synthesis. A generator G_θ with parameters θ is initialized once at the start of training. To keep server overhead small, the server runs generator training and synthesis only once every T_{gen} server updates; in intermediate rounds, it uses the latest \mathcal{D}_{KD} and proceeds directly to Step (4). In a synthesis iteration, we sample latent vectors $\mathbf{z} = \{\mathbf{z}_b\}_{b=1}^B$ and target labels $\mathbf{y}_z = \{y_b\}_{b=1}^B$ (uniformly at random over classes), and train (\mathbf{z}, θ') for K_{synth} iterations, where θ' is initialized by $\theta' \leftarrow \theta$:

$$(\mathbf{z}, \theta') \leftarrow (\mathbf{z}, \theta') - \eta_{\text{synth}} \nabla_{(\mathbf{z}, \theta')} \mathcal{L}_{\text{synth}}(G_{\theta'}(\mathbf{z})).$$

The synthesis loss is defined as:

$$\mathcal{L}_{\text{synth}} = \alpha_{\text{target}} \mathcal{L}_{\text{target}} + \alpha_{\text{feature}} \mathcal{L}_{\text{feature}} + \alpha_{\text{adv}} \mathcal{L}_{\text{adv}}. \quad (4)$$

Let $\mathbf{r}_b = G_{\theta'}(\mathbf{z}_b)$ be a synthetic input, and denote $\tilde{\mathbf{p}}_{k,b} = \sigma(\tilde{\mathbf{x}}_k(\mathbf{r}_b))$ and $\mathbf{p}_b = \sigma(\mathbf{x}^t(\mathbf{r}_b))$ as the predictive distribution of teacher k in \mathcal{C} and student (current server model), respectively. We define,

$$\begin{aligned} \mathcal{L}_{\text{target}} &= \frac{1}{B} \sum_{b=1}^B \sum_{k \in \mathcal{I}_t} \hat{\omega}_k^{y_b} \text{Cross-Entropy}(\tilde{\mathbf{p}}_{k,b}, y_b), \\ \mathcal{L}_{\text{feature}} &= \frac{1}{B} \sum_{b=1}^B \sum_{k \in \mathcal{I}_t} \hat{\omega}_k^{y_b} \|\phi(\tilde{\mathbf{x}}_k, \mathbf{r}_b) - \bar{\phi}(\tilde{\mathbf{x}}_k)\|^2, \\ \mathcal{L}_{\text{adv}} &= -\frac{1}{B} \sum_{b=1}^B \sum_{k \in \mathcal{I}_t} \hat{\omega}_k^{y_b} \mathbf{1}\{\hat{c}_{k,b} = \hat{c}_b\} \text{KL}(\tilde{\mathbf{p}}_{k,b} \parallel \mathbf{p}_b), \end{aligned}$$

where $\phi(\tilde{\mathbf{x}}_k, \mathbf{r}_b)$ extracts intermediate statistics from teacher k on input \mathbf{r}_b , and $\bar{\phi}(\tilde{\mathbf{x}}_k)$ denotes the corresponding running statistics stored in $\tilde{\mathbf{x}}_k$. The choice of ϕ depends on the modality and model architecture. Defining $\hat{c}_{k,b} = \arg \max_j (\tilde{\mathbf{p}}_{k,b})_j$ and $\hat{c}_b = \arg \max_j (\mathbf{p}_b)_j$, \mathcal{L}_{adv} discourages trivial synthetic data where the teacher and student classification match, by amplifying discrepancies. Lowest $\mathcal{L}_{\text{synth}}$ batch in K_{synth} iterations is added to the KD dataset:

$$\mathcal{D}_{\text{KD}} \leftarrow \mathcal{D}_{\text{KD}} \cup \{(\mathbf{r}_b, y_b)\}_{b=1}^B,$$

and oldest samples are discarded if \mathcal{D}_{KD} capacity is full.

(3) Meta-update of the generator. The meta-update is performed only in synthesis rounds (every T_{gen} server rounds), after Step (2). Following Fang et al. (2022), we update the meta-parameters with Reptile-style meta-learning:

$$\theta \leftarrow (1 - \lambda)\theta + \lambda\theta',$$

where $\lambda \in (0, 1)$ is the step size. Other optimizers (e.g., momentum or Adam) can also be used with the same pseudo-gradient direction $(\theta' - \theta)$ to update θ . This update ensures that G_θ gradually adapts to the changing set of teacher models without catastrophic drift, allowing the generator to retain generalizable knowledge while continuously evolving throughout the federated training process. Meta-learning thus prevents divergence and maintains stability in generating synthetic data across asynchronous, dynamic updates.

(4) Multi-teacher distillation. We distill from the buffered teachers into a student model \mathbf{x}_s , initialized as $\mathbf{x}_s \leftarrow \mathbf{x}^t$. At each distillation step, we iterate over buffered teachers $k \in \mathcal{I}_t$ and draw a teacher-aware minibatch \mathcal{B}_k from \mathcal{D}_{KD} using class-weighted sampling based on $\hat{\pi}_k$. Concretely, each element $(\mathbf{r}, y) \in \mathcal{B}_k$ is obtained by first sampling a label $y \sim \hat{\pi}_k$ and then sampling \mathbf{r} uniformly from $\{(\mathbf{r}', y') \in \mathcal{D}_{\text{KD}} : y' = y\}$. The student is trained to match teacher outputs by minimizing the average KL divergence:

$$\mathcal{L}_{\text{KD}} \triangleq \frac{1}{c} \sum_{k \in \mathcal{I}_t} \frac{1}{|\mathcal{B}_k|} \sum_{(\mathbf{r}, y) \in \mathcal{B}_k} \text{KL}(\sigma(\tilde{\mathbf{x}}_k(\mathbf{r})) \parallel \sigma(\mathbf{x}_s(\mathbf{r}))),$$

and student is updated with $\mathbf{x}_s \leftarrow \mathbf{x}_s - \eta_{\text{KD}} \nabla_{\mathbf{x}_s} \mathcal{L}_{\text{KD}}$ for K_{KD} steps. Finally, we define the distilled update as $\Delta^{\text{KD}} = \mathbf{x}_s - \mathbf{x}^t$, used in the aggregation rule Eq. (3).

2.3. Overhead Analysis

FedRevive adds server-side computation from periodic generator training and multi-teacher distillation. Relative to simple averaging step in FedAvg, this overhead is non-trivial, but it is typically comparatively small in realistic AFL deployments where client compute and communication dominate end-to-end time (Lai et al., 2021; Zhu et al., 2021a). Algorithmically, synthesis is executed only once every T_{gen} server updates and uses only K_{synth} (2 in our experiments) steps, and distillation uses K_{KD} lightweight steps (10 in our experiments). Moreover, teacher forward passes can be overlapped for buffered models with the server’s waiting for the next client upload, reducing the effective blocking time. We provide a FLOPs breakdown and discussion in Appendix C. Furthermore, to avoid any additional wall-clock delay, the server can dispatch the next local-training request immediately upon receiving an update and run synthesis, distillation, and hybrid aggregation asynchronously afterward, which hides most server compute behind client-side latency at the cost of only a small additional staleness. FedRevive has the same communication cost as FedAvg and introduces no additional memory requirement beyond standard FL except a constant-size server-side teacher buffer (Appendix H).

3. Experiments and Results

We evaluate our proposed method and baselines on both image and text classification tasks under diverse system conditions. In all experiments, we assume a large-scale FL environment consisting of 1000 clients, where only 10% are active at any time, selected uniformly at random, which reflects the intermittent availability of edge devices. To induce data heterogeneity, we follow Dirichlet partitioning (Acar et al., 2021), unless the dataset is naturally partitioned. High data heterogeneity, with concentration parameter $\alpha = 0.5$, is used in the main text experiments, and Appendix E presents results with milder heterogeneity ($\alpha = 1$).

Since our focus is on AFL, all results are presented with respect to simulated wall-clock time, which accounts for realistic computation and communication delays. To simulate system heterogeneity, we categorize clients into *slow*, *medium*, and *fast* groups according to their computation and communication speeds. Each client is assigned random delay parameters based on its group. When a client participates in training, its local computation and communication durations are sampled from its random generator, ensuring stochastic time variations across rounds. This setup provides system heterogeneity across clients and rounds, reflecting real environments. Additional details on time-simulation and staleness distribution plot are given in Appendix D.

All reported results are averaged over three random seeds, with shaded regions indicating the standard error. For every compared method, we tune hyperparameters on validation performance. Since asynchronous algorithms tend to exhibit fluctuating behavior, we report running-average performance until peak performance is reached for clearer visualization. Unprocessed results are provided in Appendix F.

3.1. Datasets, Models, and Baselines

We benchmark our method on both image and text classification tasks using the following datasets and models:

- **CIFAR-10 and CIFAR-100:** 10 and 100-class RGB image classification tasks. We train ResNet-18 architecture with 11.2M parameters (He et al., 2016).
- **FEMNIST:** The Federated Extended MNIST (FEMNIST) dataset (Caldas et al., 2019) is a 62-class grayscale handwritten character classification task. It provides a natural user-level partition across approximately 3500 writers. We adopt a multi-layer convolutional neural network (CNN) model with 421k parameters.
- **20NewsGroups:** 20-class text topic classification for news using a pretrained T5-small (Raffel et al., 2023) transformer model with 35.6M parameters.

Except for FEMNIST, we simulate 1000 clients by repeatedly sampling the dataset to allocate 350 samples per client. For FEMNIST, we randomly select 1000 users from the natural partition, each corresponding to an individual client.

We compare our proposed FedRevive with representative baselines from the literature as summarized below:

- **FedAvg:** The vanilla synchronous FL algorithm (McMahan et al., 2017). The server waits for all active clients every round before aggregation, which eliminates staleness, but round time can be dominated by stragglers (Xie et al., 2019).
- **FedBuff (Eq. (2)):** A buffered asynchronous variant of FedAvg (Nguyen et al., 2022). The server accumulates incoming client updates in a buffer and aggregates once the buffer is full. When the buffer size is 1, FedBuff reduces to standard asynchronous FedAvg (Xie et al., 2019) in Eq. (1).

Since we tune the buffer size including 1, we report stronger FedBuff as the representative asynchronous baseline.

- **FedRevive (Eq. (3)):** Our proposed method. $K_{\text{synth}} = 2$, $K_{\text{KD}} = T_{\text{gen}} = 10$, and $c = 8$ are used in all experiments.
- **DD-FedRevive:** A fully equipped ablation variant, Data-Driven-FedRevive, where the server has access to a disjoint auxiliary dataset with size of 16.7% of the total training samples across clients, sampled from the overall client distribution. KD is performed directly on this data, i.e. FedRevive without generator-based synthesis. DD-FedRevive assumes client label proportions are known in this variant rather than estimated. This setting is included only for ablation due to its impractical assumptions.
- **AFL-DW:** Prior asynchronous FL work (Chen et al., 2019; Shi et al., 2020; Lu et al., 2020) down-weights stale updates to mitigate their adverse effect. To test if FedRevive improves performance mainly due to the KD update rather than only reducing stale-update impact in Eq. (3), we include AFL-Down Weighting (AFL-DW) as ablation that only down-weights regular update, without any synthesis or distillation. Concretely, we modify Eq. (3) to $\mathbf{x}^{(t+1)} \leftarrow \mathbf{x}^{(t)} + \eta_s (1 - \beta(\tau_i^t)) \Delta_i$, while keeping all other hyperparameters and $\beta(\cdot)$ choice identical to FedRevive.

Hyperparameters and β Function Selection For each compared method, we tune hyperparameters individually on each task. For FedRevive and DD-FedRevive, the weighting function β in Eq. (3) controls the mix between the parameter-space update and the KD update. When the received client update has low staleness, the server should rely more on parameter-space aggregation, whereas for highly stale updates, the KD component should be emphasized. We consider several monotone scheduling families for β (Figure 11) and use the $1 - \text{cosine}$ function in all experiments. Full hyperparameter settings are provided in Appendix I.

3.2. Main Results and Ablation Experiments

We provide main experiments’ training curves in Figure 2, and test accuracy and time-to-target results in Table 1.

Image task results. For CIFAR-10, CIFAR-100, and FEMNIST, the synthesis module in FedRevive uses the same lightweight generator architecture as Fang et al. (2022), which maps latent noise to an image input via a linear projection followed by a CNN block. In all experiments, synchronous baseline FedAvg incurs a long wall-clock time because the server waits for all selected clients, which limits practical convergence speed even though it avoids staleness.

In CIFAR-10, FedRevive reaches a higher final accuracy than FedBuff while converging faster, despite operating under the same asynchrony. This gain comes from continually transferring knowledge from buffered stale client models

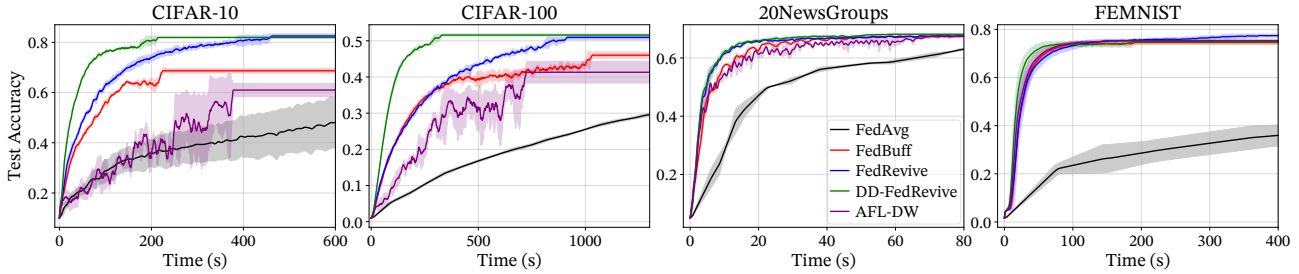


Figure 2. Test accuracy versus simulated time on CIFAR-10, CIFAR-100, 20NewsGroups, and FEMNIST. On CIFAR-10, FedRevive converges faster and reaches a higher final accuracy than the asynchronous baseline FedBuff. On the harder CIFAR-100 task, the gap between FedRevive and FedBuff becomes more pronounced later in training, when client models provide stronger teachers. On 20NewsGroups, FedRevive achieves faster convergence than FedBuff. On FEMNIST, all asynchronous methods exhibit similar overall convergence due to the relative simplicity of the task, but FedRevive still achieves higher accuracy than the baselines.

through DFKD, so each received update contributes more effectively than parameter aggregation alone. Ablation variant DD-FedRevive, which assumes access to a small public dataset for distillation, exhibits the fastest convergence due to the immediate availability of real data. However, FedRevive surpasses DD-FedRevive in final performance, as the fixed public dataset in DD-FedRevive may lead to partial overfitting, while the synthetic data in FedRevive adaptively evolves alongside the training, yielding richer and more diverse knowledge transfer. Finally, the performance of AFL-DW remains considerably lower than that of FedRevive, confirming that the improvement of our method arises not primarily from down-weighting stale updates but from the proposed DFKD mechanism itself.

On the harder CIFAR-100 task with 100 classes, class-conditioned synthesis and distillation are more challenging, especially during early training when the teachers are not trained well. Once client models become sufficiently accurate, the advantage of FedRevive becomes clearer and the gap with FedBuff widens. The ablation variant DD-FedRevive converges fastest due to immediate access to real server-side data and client label proportions. In terms of final accuracy, FedRevive outperforms the baselines. Finally, on FEMNIST, stale updates are less detrimental, likely due to simpler visual patterns, so asynchronous baselines exhibit similar convergence behavior. Even in this regime, FedRevive still improves the final performance.

Text task results. For the text-domain task, 20NewsGroups, we adopt the T5-small architecture (Raffel et al., 2023) as the backbone and attach a lightweight classification head composed of linear layers. The head reads the final hidden state of a prepended dummy prediction token and outputs class logits. We truncate inputs to length 128 after adding this token.

To accommodate discrete text inputs, we replace the image generator with a prompt-based synthesis mechanism. Unlike images, text lies in a discrete and highly structured space,

and prior data-free distillation for language often relies on external or generated corpora (Palo et al., 2024; Xu et al., 2024; Tian et al., 2025). In FedRevive, instead of training a generator network, we meta-learn four soft prompt vectors inserted immediately after the prediction token, following soft prompt learning (Lester et al., 2021; Gu et al., 2022). The remaining prompt embeddings are initialized for training using short synthetic snippets produced by a small (1B params) instruction-tuned language model (Zhang et al., 2024) with a high decoding temperature.

Figure 2 (third panel) shows test accuracy versus simulated time on 20NewsGroups. FedRevive consistently improves convergence speed among baselines. In this setting, AFL-DW performs similarly to FedBuff, while FedRevive and DD-FedRevive converge the fastest.

We verify that these LM-generated snippets do not provide meaningful task leakage. Specifically, centralized training on only the generated synthetic data achieves a best test accuracy of $48.08\% \pm 0.22\%$ on 20NewsGroups, which is far below the federated performance of all methods reported in Table 1. This indicates that the generated snippets only serve as a weak linguistic prior and a neutral initialization that stabilizes the synthetic optimization, rather than a source of usable task data. In this setup, the generator parameters θ correspond to four meta-learned soft prompt vectors, while the latent variable \mathbf{z} denotes the remaining embedding vectors initialized from the synthetic snippets.

Robustness to shift in delay schemes. All main experiments use a fixed stochastic delay model for client-side computation and communication (details in Section D), which induces a long-tailed staleness distribution in Figure 6. We tune all hyperparameters under this default delay scheme. To test robustness to system changes, we re-run the asynchronous methods on CIFAR-10 and 20NewsGroups under an alternative delay schedule that shifts the induced staleness distribution (see Figure 7 in Appendix D.1). Importantly, we do not re-tune any hyperparameters. Figure 3 shows that

Table 1. Final test accuracy and time-to-target reported as accuracy% (time), where accuracy is the mean final test accuracy, and (time) shows the mean simulated time to reach 85% of best FedBuff accuracy. For each dataset, the best two accuracy and (time) values are highlighted in bold. FedRevive achieves substantially faster convergence than baseline FedBuff, demonstrating up to 38.4% shorter time-to-target. Furthermore, FedRevive achieves higher final accuracy than FedBuff with up to 16.5% increase. The variant DD-FedRevive, which assumes access to a small public dataset and client class proportions, attains the fastest convergence overall but remains only a hypothetical upper bound due to its unrealistic assumptions.

Method	CIFAR-10	CIFAR-100	20NewsGroups	FEMNIST
FedAvg	63.18 (675.8)	45.73 (2957.0)	68.46 (53.4)	63.62 (>1000)
FedBuff	63.99 (96.4)	43.13 (318.9)	67.46 (9.9)	73.92 (38.2)
AFL-DW	45.79 (184.7)	32.47 (451.5)	66.98 (10.8)	74.63 (35.3)
DD-FedRevive	78.32 (28.6)	49.17 (101.6)	67.48 (6.2)	74.11 (25.4)
FedRevive	80.51 (65.5)	49.01 (304.6)	67.09 (6.1)	77.03 (34.7)

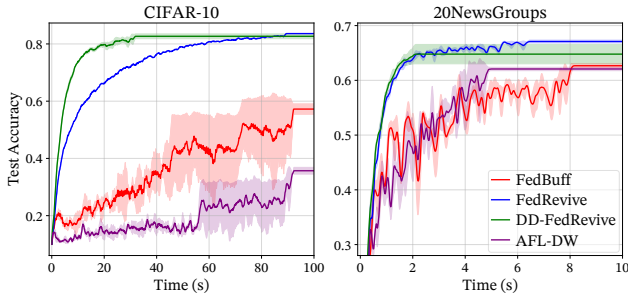


Figure 3. **Robustness under a shifted delay schedule.** Test accuracy vs. simulated time on CIFAR-10 and 20NewsGroups using an alternative delay scheme that shifts the staleness distribution. Hyperparameters are tuned under the default delay model. FedRevive is robust to the change while baselines perform worse.

the DFKD-based methods (FedRevive and DD-FedRevive) remain substantially more robust to this delay shift, while asynchronous baselines (e.g., FedBuff and AFL-DW) exhibit slower convergence and degraded final accuracy under the shifted staleness regime.

Update contributions in DFKD. To isolate the contribution of each update component in Eq. (3) and to study the role of the staleness-dependent mixing schedule $\beta(\tau)$, we run FedRevive on CIFAR-10. At each server round, we separately apply (i) only the stale client update $\Delta_i^{(t-\tau_i^t)}$, (ii) only the KD-revived update Δ_i^{KD} produced by KD-Revive(\cdot), and (iii) their combined update as in Eq. (3). We repeat this under three mixing regimes: the adaptive schedule used in the main experiments, and two fixed schedules with $\beta(\tau) = 0.75$ and $\beta(\tau) = 1$. Figure 4 (left) shows that the KD-revived update produces large improvements and proves the effectiveness of our method. However, these per-update effects do not imply that one can rely on KD alone in training. Figure 4 (right) compares training curves under adaptive $\beta(\tau)$ versus constant β . Constant high β , 0.75 or 1, reduces the contribution of the original client updates and leads to worse performance, showing that sustained progress requires accumulating client-side learning across rounds. Additional diagnostics that decom-

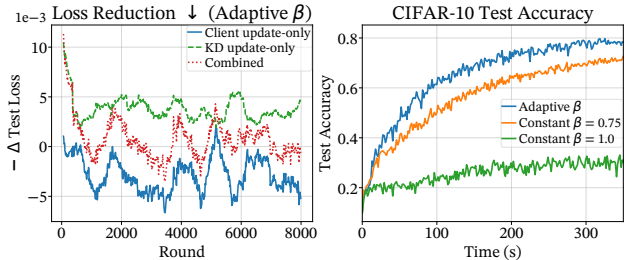


Figure 4. **Update contributions and the role of $\beta(\tau)$ on CIFAR-10.** **Left:** per-round effect of applying only the stale client update, only the KD-revived update, or their combination under the adaptive $\beta(\tau)$ schedule. **Right:** test accuracy vs. simulated time under adaptive and constant (0.75 and 1) $\beta(\tau)$. Constant schedules underweight the client update and degrade performance.

pose improvement by update components are provided in Appendix G, where the benefit of adaptive β is visible.

4. Conclusion

Asynchronous federated learning algorithms offer the scalability required for large-scale decentralized training and cross-device FL, yet suffer from staleness. Although stale updates can hinder convergence, they still contain valuable information about the clients’ local data. We introduce FedRevive, a scalable asynchronous FL framework that extracts and utilizes this information through data-free knowledge distillation. By combining lightweight meta-learned synthetic data generation with multi-teacher distillation, our approach effectively mitigates staleness while preserving data privacy and system efficiency. Experiments on vision and text tasks demonstrate that FedRevive significantly improves convergence speed and final accuracy over baselines. Extending FedRevive with pretrained generative models for applicable data modalities presents a promising direction.

Acknowledgements

This work was partially supported by the US National Science Foundation under grants CNS-2106891 and CNS-2409138 to CJW and CCF 2045694, CNS-2112471, CPS-2111751, and ONR N00014-23-1-2149 to GJ.

References

- Acar, D. A. E., Zhao, Y., Matas, R., Mattina, M., Whatmough, P., and Saligrama, V. Federated learning based on dynamic regularization. In *International Conference on Learning Representations*, 2021. URL <https://openreview.net/forum?id=B7v4QMR6Z9w>.
- Askin, B., Sharma, P., Joe-Wong, C., and Joshi, G. Fedast: federated asynchronous simultaneous training. In *Proceedings of the Fortieth Conference on Uncertainty in Artificial Intelligence*, UAI '24. JMLR.org, 2024.
- Bonawitz, K. A., Eichner, H., Grieskamp, W., Huba, D., Ingerman, A., Ivanov, V., Kiddon, C., Konečný, J., Mazzocchi, S., McMahan, H. B., Overveldt, T. V., Petrou, D., Ramage, D., and Roselander, J. Towards federated learning at scale: System design. *CoRR*, abs/1902.01046, 2019. URL <http://arxiv.org/abs/1902.01046>.
- Caldas, S., Duddu, S. M. K., Wu, P., Li, T., Konečný, J., McMahan, H. B., Smith, V., and Talwalkar, A. Leaf: A benchmark for federated settings, 2019. URL <https://arxiv.org/abs/1812.01097>.
- Chen, M., Mao, B., and Ma, T. Fedsta: A staleness-aware asynchronous federated learning algorithm with non-iid data. *Future Generation Computer Systems*, 120:1–12, 2021.
- Chen, Y., Sun, X., and Jin, Y. Communication-efficient federated deep learning with layerwise asynchronous model update and temporally weighted aggregation. *IEEE transactions on neural networks and learning systems*, 31(10):4229–4238, 2019.
- Chen, Y., Ning, Y., Slawski, M., and Rangwala, H. Asynchronous Online Federated Learning for Edge Devices with Non-IID Data. In *2020 IEEE International Conference on Big Data (Big Data)*, pp. 15–24, Los Alamitos, CA, USA, December 2020. IEEE Computer Society. doi: 10.1109/BigData50022.2020.9378161. URL <https://doi.ieeecomputersociety.org/10.1109/BigData50022.2020.9378161>.
- Cui, H., Cipar, J., Ho, Q., Kim, J. K., Lee, S., Kumar, A., Wei, J., Dai, W., Ganger, G. R., Gibbons, P. B., et al. Exploiting bounded staleness to speed up big data analytics. In *USENIX Annual Technical Conference (ATC)*, pp. 37–48, 2014.
- Dean, J. et al. Large scale distributed deep networks. In *Advances in Neural Information Processing Systems*, pp. 1223–1231, 2012.
- Dutta, S., Joshi, G., Ghosh, S., Dube, P., and Nagpurkar, P. Slow and Stale Gradients Can Win the Race: Error-Runtime Trade-offs in Distributed SGD. *Proceedings of the International Conference on Artificial Intelligence and Statistics (AISTATS)*, April 2018.
- Fan, B., Jiang, S., Su, X., Tarkoma, S., and Hui, P. A Survey on Model-heterogeneous Federated Learning: Problems, Methods, and Prospects. In *2024 IEEE International Conference on Big Data (BigData)*, pp. 7725–7734, Los Alamitos, CA, USA, December 2024. IEEE Computer Society. doi: 10.1109/BigData62323.2024.10825769. URL <https://doi.ieeecomputersociety.org/10.1109/BigData62323.2024.10825769>.
- Fang, G., Mo, K., Wang, X., Song, J., Bei, S., Zhang, H., and Song, M. Up to 100x faster data-free knowledge distillation. *Proceedings of the AAAI Conference on Artificial Intelligence*, 36(6):6597–6604, Jun. 2022. doi: 10.1609/aaai.v36i6.20613. URL <https://ojs.aaai.org/index.php/AAAI/article/view/20613>.
- Gao, L., Zhang, Z., and Wu, C. Feddtg: federated data-free knowledge distillation via three-player generative adversarial networks, 2025. URL <https://arxiv.org/abs/2201.03169>.
- Gu, Y., Han, X., Liu, Z., and Huang, M. PPT: Pre-trained prompt tuning for few-shot learning. In Muresan, S., Nakov, P., and Villavicencio, A. (eds.), *Proceedings of the 60th Annual Meeting of the Association for Computational Linguistics (Volume 1: Long Papers)*, pp. 8410–8423, Dublin, Ireland, May 2022. Association for Computational Linguistics. doi: 10.18653/v1/2022.acl-long.576. URL <https://aclanthology.org/2022.acl-long.576/>.
- Gupta, S., Zhang, W., and Wang, F. Model accuracy and runtime tradeoff in distributed deep learning: A systematic study. In *International Conference on Data Mining*, pp. 171–180, 2016.
- He, K., Zhang, X., Ren, S., and Sun, J. Deep residual learning for image recognition. In *Proceedings of the IEEE conference on computer vision and pattern recognition*, pp. 770–778, 2016.
- Hinton, G. E., Vinyals, O., and Dean, J. Distilling the knowledge in a neural network. *CoRR*, abs/1503.02531, 2015. URL <http://arxiv.org/abs/1503.02531>.
- Ho, Q., Cipar, J., Cui, H., Lee, S., Kim, J. K., Gibbons, P. B., Gibson, G. A., Ganger, G., and Xing, E. P. More effective

- distributed ml via a stale synchronous parallel parameter server. In *Advances in Neural Information Processing Systems*, pp. 1223–1231, 2013.
- Itahara, S., Nishio, T., Koda, Y., Morikura, M., and Yamamoto, K. Distillation-based semi-supervised federated learning for communication-efficient collaborative training with non-iid private data. *IEEE Transactions on Mobile Computing*, 22(1):191–205, 2021.
- Jiao, X., Yin, Y., Shang, L., Jiang, X., Chen, X., Li, L., Wang, F., and Liu, Q. TinyBERT: Distilling BERT for natural language understanding. In Cohn, T., He, Y., and Liu, Y. (eds.), *Findings of the Association for Computational Linguistics: EMNLP 2020*, pp. 4163–4174, Online, November 2020. Association for Computational Linguistics. doi: 10.18653/v1/2020.findings-emnlp.372. URL <https://aclanthology.org/2020.findings-emnlp.372/>.
- Koloskova, A., Stich, S. U., and Jaggi, M. Sharper convergence guarantees for asynchronous sgd for distributed and federated learning. *Advances in Neural Information Processing Systems*, 35:17202–17215, 2022.
- Lai, F., Dai, Y., Zhu, X., Madhyastha, H. V., and Chowdhury, M. FedScale: Benchmarking model and system performance of federated learning. In *Proceedings of the First Workshop on Systems Challenges in Reliable and Secure Federated Learning, ResilientFL ’21*, pp. 1–3, New York, NY, USA, 2021. Association for Computing Machinery. ISBN 9781450387088. doi: 10.1145/3477114.3488760. URL <https://doi.org/10.1145/3477114.3488760>.
- Lee, S., Yoo, K., and Kwak, N. Edge bias in federated learning and its solution by buffered knowledge distillation. *arXiv preprint arXiv:2010.10338*, 2020.
- Lester, B., Al-Rfou, R., and Constant, N. The power of scale for parameter-efficient prompt tuning. In Moens, M.-F., Huang, X., Specia, L., and Yih, S. W.-t. (eds.), *Proceedings of the 2021 Conference on Empirical Methods in Natural Language Processing*, pp. 3045–3059, Online and Punta Cana, Dominican Republic, November 2021. Association for Computational Linguistics. doi: 10.18653/v1/2021.emnlp-main.243. URL <https://aclanthology.org/2021.emnlp-main.243/>.
- Li, D. and Wang, J. Fedmd: Heterogenous federated learning via model distillation, 2019. URL <https://arxiv.org/abs/1910.03581>.
- Li, L., Gou, J., Yu, B., Du, L., and Tao, Z. Y. D. Federated distillation: A survey. *arXiv preprint arXiv:2404.08564*, 2024.
- Lian, X., Huang, Y., Li, Y., and Liu, J. Asynchronous parallel stochastic gradient for nonconvex optimization. In *Advances in Neural Information Processing Systems*, pp. 2737–2745, 2015.
- Lin, T., Kong, L., Stich, S. U., and Jaggi, M. Ensemble distillation for robust model fusion in federated learning. *Advances in neural information processing systems*, 33: 2351–2363, 2020.
- Lopes, R. G., Fenu, S., and Starner, T. Data-free knowledge distillation for deep neural networks, 2017. URL <https://arxiv.org/abs/1710.07535>.
- Lu, C., Sun, Y., Li, P., and Yang, Z. Corrected with the latest version: Make robust asynchronous federated learning possible, 2025. URL <https://arxiv.org/abs/2504.04081>.
- Lu, X., Liao, Y., Lio, P., and Hui, P. Privacy-preserving asynchronous federated learning mechanism for edge network computing. *IEEE Access*, 8:48970–48981, 2020. doi: 10.1109/ACCESS.2020.2978082.
- Luo, B., Xiao, W., Wang, S., Huang, J., and Tassiulas, L. Tackling system and statistical heterogeneity for federated learning with adaptive client sampling. In *IEEE INFOCOM 2022 - IEEE Conference on Computer Communications*, pp. 1739–1748. IEEE Press, 2022. doi: 10.1109/INFOCOM48880.2022.9796935. URL <https://doi.org/10.1109/INFOCOM48880.2022.9796935>.
- Mansourian, A. M., Ahmadi, R., Ghafouri, M., Babaei, A. M., Golezani, E. B., yasamani ghamchi, Z., Ramezani, V., Taherian, A., Dinashi, K., Miri, A., and Kasaei, S. A comprehensive survey on knowledge distillation. *Transactions on Machine Learning Research*, 2025. ISSN 2835-8856. URL <https://openreview.net/forum?id=3cbJzdR78B>.
- McMahan, B., Moore, E., Ramage, D., Hampson, S., and Arcas, B. A. y. Communication-Efficient Learning of Deep Networks from Decentralized Data. In Singh, A. and Zhu, J. (eds.), *Proceedings of the 20th International Conference on Artificial Intelligence and Statistics*, volume 54 of *Proceedings of Machine Learning Research*, pp. 1273–1282. PMLR, 20–22 Apr 2017. URL <https://proceedings.mlr.press/v54/mcmahan17a.html>.
- Mitliagkas, I., Zhang, C., Hadjis, S., and Ré, C. Asynchrony begets momentum, with an application to deep learning. In *Allerton Conference on Communication, Control, and Computing*, pp. 997–1004. IEEE, 2016.
- Nguyen, J., Malik, K., Zhan, H., Yousefpour, A., Rabbat, M., Malek, M., and Huba, D. Federated learning with

- buffered asynchronous aggregation. In Camps-Valls, G., Ruiz, F. J. R., and Valera, I. (eds.), *Proceedings of The 25th International Conference on Artificial Intelligence and Statistics*, volume 151 of *Proceedings of Machine Learning Research*, pp. 3581–3607. PMLR, 28–30 Mar 2022. URL <https://proceedings.mlr.press/v151/nguyen22b.html>.
- Nichol, A., Achiam, J., and Schulman, J. On first-order meta-learning algorithms. *arXiv preprint arXiv:1803.02999*, 2018.
- Palo, F. D., Singhi, P., and Fadlallah, B. H. Performance-guided LLM knowledge distillation for efficient text classification at scale. In Al-Onaizan, Y., Bansal, M., and Chen, Y.-N. (eds.), *Proceedings of the 2024 Conference on Empirical Methods in Natural Language Processing*, pp. 3675–3687, Miami, Florida, USA, November 2024. Association for Computational Linguistics. doi: 10.18653/v1/2024.emnlp-main.215. URL <https://aclanthology.org/2024.emnlp-main.215/>.
- Qin, L., Zhu, T., Zhou, W., and Yu, P. S. Knowledge distillation in federated learning: a survey on long lasting challenges and new solutions, 2024. URL <https://arxiv.org/abs/2406.10861>.
- Raffel, C., Shazeer, N., Roberts, A., Lee, K., Narang, S., Matena, M., Zhou, Y., Li, W., and Liu, P. J. Exploring the limits of transfer learning with a unified text-to-text transformer, 2023. URL <https://arxiv.org/abs/1910.10683>.
- Richtarik, P. Handling device heterogeneity in federated learning: The first optimal parallel sgd in the presence of data, compute and communication heterogeneity. In *Proceedings of the International Workshop on Secure and Efficient Federated Learning*, pp. 1–1, 2025.
- Rieke, N., Hancox, J., Li, W., Milletari, F., Roth, H. R., Albarqouni, S., Bakas, S., Galtier, M. N., Landman, B. A., Maier-Hein, K., et al. The future of digital health with federated learning. *NPJ digital medicine*, 3(1):119, 2020.
- Shang, E., Liu, H., Yang, Z., Du, J., and Ge, Y. Fedbikd: Federated bidirectional knowledge distillation for distracted driving detection. *IEEE Internet of Things Journal*, 10(13):11643–11654, 2023. doi: 10.1109/JIOT.2023.3243622.
- Shi, G., Li, L., Wang, J., Chen, W., Ye, K., and Xu, C. Hysync: Hybrid federated learning with effective synchronization. In *2020 IEEE 22nd International Conference on High Performance Computing and Communications; IEEE 18th International Conference on Smart City; IEEE 6th International Conference on Data Science and Systems (HPCC/SmartCity/DSS)*, pp. 628–633, 2020. doi: 10.1109/HPCC-SmartCity-DSS50907.2020.00080.
- Tian, Y., Han, Y., Chen, X., Wang, W., and Chawla, N. V. Beyond answers: Transferring reasoning capabilities to smaller llms using multi-teacher knowledge distillation. In *Proceedings of the Eighteenth ACM International Conference on Web Search and Data Mining, WSDM ’25*, pp. 251–260, New York, NY, USA, 2025. Association for Computing Machinery. ISBN 9798400713293. doi: 10.1145/3701551.3703577. URL <https://doi.org/10.1145/3701551.3703577>.
- Xie, C., Koyejo, S., and Gupta, I. Asynchronous federated optimization. *arXiv preprint arXiv:1903.03934*, 2019.
- Xu, C., Qu, Y., Xiang, Y., and Gao, L. Asynchronous federated learning on heterogeneous devices: A survey. *Computer Science Review*, 50:100595, 2023. ISSN 1574-0137. doi: <https://doi.org/10.1016/j.cosrev.2023.100595>. URL <https://www.sciencedirect.com/science/article/pii/S157401372300062X>.
- Xu, X., Li, M., Tao, C., Shen, T., Cheng, R., Li, J., Xu, C., Tao, D., and Zhou, T. A survey on knowledge distillation of large language models, 2024. URL <https://arxiv.org/abs/2402.13116>.
- Yang, Q., Liu, Y., Chen, T., and Tong, Y. Federated machine learning: Concept and applications. *ACM Transactions on Intelligent Systems and Technology (TIST)*, 10(2):1–19, 2019.
- Yu, X., Cherkasova, L., Vardhan, H., Zhao, Q., Ekaireb, E., Zhang, X., Mazumdar, A., and Rosing, T. Async-hfl: Efficient and robust asynchronous federated learning in hierarchical iot networks. In *Proceedings of the 8th ACM/IEEE Conference on Internet of Things Design and Implementation*, pp. 236–248, 2023.
- Zagoruyko, S. and Komodakis, N. Paying more attention to attention: Improving the performance of convolutional neural networks via attention transfer. In *International Conference on Learning Representations*, 2017.
- Zhang, L., Shen, L., Ding, L., Tao, D., and Duan, L.-Y. Fine-tuning global model via data-free knowledge distillation for non-iid federated learning. In *Proceedings of the IEEE/CVF conference on computer vision and pattern recognition*, pp. 10174–10183, 2022.
- Zhang, P., Zeng, G., Wang, T., and Lu, W. Tinyllama: An open-source small language model, 2024.
- Zhang, W., Gupta, S., Lian, X., and Liu, J. Staleness-aware async-sgd for distributed deep learning. In *International Joint Conference on Artificial Intelligence*, pp. 2350–2356. AAAI Press, 2016.

Zhu, L., Lin, H., Lu, Y., Lin, Y., and Han, S. Delayed gradient averaging: Tolerate the communication latency for federated learning. In Beygelzimer, A., Dauphin, Y., Liang, P., and Vaughan, J. W. (eds.), *Advances in Neural Information Processing Systems*, 2021a. URL <https://openreview.net/forum?id=ACFHNxVNvfk>.

Zhu, Z., Hong, J., and Zhou, J. Data-free knowledge distillation for heterogeneous federated learning. In *International conference on machine learning*, pp. 12878–12889. PMLR, 2021b.

A. Extended Related Work

Synchronous FL. Since the seminal work of McMahan et al. (2017), FL has proven effective for collaboratively training models from decentralized and private data sources. Most existing FL algorithms employ *synchronous* aggregation, where the server waits for all selected clients to complete their local training and then averages their model updates. However, this synchronization scheme creates a major bottleneck. In realistic environments, edge devices exhibit high variability in computation and communication capabilities (e.g., mobile phones versus embedded edge devices, Wi-Fi versus cellular connections), resulting in widely varying local training times. Consequently, in each round, the server must wait for the slowest client (the “straggler”), leaving faster clients idle and underutilized. Several methods have been proposed to alleviate the straggler problem, such as aggregating only the updates that arrive before a predetermined time (Bonawitz et al., 2019) or randomly subsampling available clients (Luo et al., 2022). However, these approaches can bias training toward inherently faster clients and still underutilize slower ones. The straggler issue is further exacerbated in large-scale deployments, where the growing number of clients increases the likelihood of slow update returns and communication delays (Yu et al., 2023). As a result, synchronous aggregation inherently limits scalability and resource efficiency in federated networks.

Asynchronous FL. To overcome the straggler bottleneck and scalability issues of synchronous aggregation, a growing body of work has explored *asynchronous FL* (AFL) (Xie et al., 2019; Xu et al., 2023; Nguyen et al., 2022; Chen et al., 2020; Richtarik, 2025; Nichol et al., 2018). AFL builds upon a line of previous works on asynchronous distributed stochastic gradient descent (SGD) in the data-center setting (Dean et al., 2012; Gupta et al., 2016; Cui et al., 2014; Ho et al., 2013; Lian et al., 2015; Zhang et al., 2016; Mitliagkas et al., 2016; Dutta et al., 2018). In AFL, the server integrates client updates as soon as they arrive, either individually or in small mini-batches, without waiting for global synchronization. This design enables faster convergence by mitigating the straggler effect and improving resource utilization. However, asynchronicity introduces a new challenge: *stale updates*. Because clients train on outdated versions of the global model, their updates may become obsolete by the time they reach the server. Incorporating these stale updates can inject inconsistency or even destabilize training (Xu et al., 2023).

To mitigate staleness, several strategies have been proposed. Nguyen et al. (2022) employ buffer for incoming updates and averages them before aggregation, which smooths model update frequency and reduces variance within the server updates due to data heterogeneity despite the cost of slower server updates. Another line of work assigns lower weights to stale updates as a function of their staleness (Chen et al., 2019; Shi et al., 2020; Lu et al., 2020; Zhang et al., 2016; Dutta et al., 2018; Cui et al., 2014), reducing the influence of outdated gradients but potentially discarding valuable information from slower clients. Importantly, each client’s update encapsulates rich information about its local data distribution. In AFL, the challenge lies in how to effectively utilize this information despite staleness. In our work, we leverage DFKD to extract and transfer the informative content from stale client updates to the current server model.

KD and DFKD. KD is a powerful technique for transferring learned representations of a better-performing *teacher* model to a *student* (Hinton et al., 2015). The standard formulation trains the student to mimic the teacher’s output logits, which encode class probabilities, inter-class similarity, and uncertainty. KD has since been widely adopted across various modalities, including vision, speech, and natural language processing, where it consistently improves generalization and model compactness (Mansourian et al., 2025; Zagoruyko & Komodakis, 2017; Jiao et al., 2020). The vanilla KD framework, however, fundamentally requires access to a dataset on which both teacher and student are evaluated during distillation. In many practical cases, such as privacy-preserving learning or FL, direct access to data is unavailable, making conventional KD infeasible. This has motivated the emergence of DFKD (Lopes et al., 2017), which aims to perform distillation without real data. Methods typically optimize a generator or latent codes to synthesize pseudo-samples under objectives that align teacher predictions, match intermediate statistics (e.g., batch statistics), or introduce adversarial criteria to amplify teacher–student discrepancies (Mansourian et al., 2025; Lopes et al., 2017; Fang et al., 2022). Then, these samples are utilized for distillation.

KD and DFKD in FL. KD has also been incorporated into the FL paradigm for various purposes, such as mitigating client bias and data heterogeneity, enabling architecture-heterogeneous models, and enhancing data privacy (Li et al., 2024; Li & Wang, 2019; Lin et al., 2020; Qin et al., 2024; Fan et al., 2024). In FL, KD can be performed on either the *server side*, where the global model distills knowledge from client models (Lee et al., 2020; Li & Wang, 2019), or on the *client side*, where clients distill knowledge from the server model or peer models (Itahara et al., 2021; Shang et al., 2023). While some of these methods assume the presence of a shared public dataset for knowledge transfer (Itahara et al., 2021), some approaches adopt DFKD to remove this dependency (Gao et al., 2025; Zhang et al., 2022; Zhu et al., 2021b). However, existing works applying KD or DFKD have been primarily designed for *synchronous* FL, and the use of KD in *asynchronous* FL remains

largely unexplored. The few existing efforts (Lu et al., 2025) rely on the unrealistic assumption of public data availability. In this work, we leverage DFKD in the asynchronous FL setting to enhance both scalability and convergence stability.

B. Deriving Client Class-Proportion Proxies

FedRevive uses proxy per-client class-proportion vectors to (i) construct client-conditioned synthesis targets and (ii) perform class-aware multi-teacher distillation. To avoid requiring access to private client label histograms, we derive a coarse per-client class-proportion proxy on the server using only the first few *regular* model updates (no extra client computation, metadata, or communication).

Deriving class-proportion proxies from early uploads. Let $\mathbf{y}_i^{(u)}$ denote the u -th model upload received from client i (ordered by server reception). We find proxy class proportions from the first $T_{\text{est}} = 2$ uploads. For each upload $\mathbf{y}_i^{(u)}$, the server probes the model with a batch of random inputs \mathbf{r} and computes

$$\tilde{\pi}_i^{(u)} = (1/|\mathbf{r}|) \sum_{r \in \mathbf{r}} \sigma(\mathbf{y}_i^{(u)}(r)/T_{\text{probe}}), \quad u = 1, \dots, T_{\text{est}},$$

where $\sigma(\cdot)$ is the softmax function. For vision models, r is i.i.d. Gaussian noise with the same input shape as the model. For language models, r is a random token sequence with the same length as the model input (tokens sampled uniformly from the vocabulary). The final proxy is the average across early uploads,

$$\hat{\pi}_i = (1/T_{\text{est}}) \sum_{u=1}^{T_{\text{est}}} \tilde{\pi}_i^{(u)},$$

and is fixed for the remainder of training. We use random-input probing as a weak-signal heuristic: local training generally induces class-dependent logit biases. As a result, even under out-of-distribution probes (Gaussian noise for vision, random tokens for text), the model’s predictive distribution is not arbitrary; it is typically closer to uniform when the client’s label histogram is near-uniform, and becomes increasingly skewed toward the majority classes as the client’s data become more imbalanced. We do not claim this yields exact histograms, but only a coarse ranking of dominant classes, which we find sufficient to weight buffered teachers.

This estimation is performed online as uploads arrive and requires only server-side forward passes. We apply temperature scaling in the probing softmax. We use $T_{\text{probe}} = 0.8$ on CIFAR-10, $T_{\text{probe}} = 1$ on CIFAR-100, $T_{\text{probe}} = 1.4$ on FEMNIST, and $T_{\text{probe}} = 1.6$ on 20NewsGroups.

Proxy quality. For analysis only, we compare the proxy $\hat{\pi}_i$ against the ground-truth client label distribution π_i via $D_{\text{KL}}(\pi_i \parallel \hat{\pi}_i)$. For each seed, we compute the mean KL across all clients ($N = 1000$), then report mean \pm std across seeds in Table 2.

Table 2. KL divergence between true client label proportions and the server-derived proxy proportions, reported as mean \pm std across seeds. We report the average client KL after the second received update.

Dataset	Average $D_{\text{KL}}(\pi_i \parallel \hat{\pi}_i)$
CIFAR-10	0.4240 \pm 0.0103
CIFAR-100	0.5539 \pm 0.0174
20NewsGroups	0.5889 \pm 0.0312
FEMNIST	0.4561 \pm 0.0554

Sensitivity to label-proportion estimation errors. While the probing-based proxy is only a coarse heuristic, it is designed to recover *relative* class dominance rather than exact client histograms. To evaluate whether estimation errors affect FedRevive, we run an ablation where the class-aware teacher weighting uses either the estimated proportions or the ground-truth client label proportions (just for an ablation purpose). As shown in Fig. 5, using estimated proportions matches the training dynamics and final accuracy across CIFAR-10, CIFAR-100, and FEMNIST, indicating that FedRevive is not overly sensitive to estimation noise and mainly benefits from a rough identification of dominant classes.

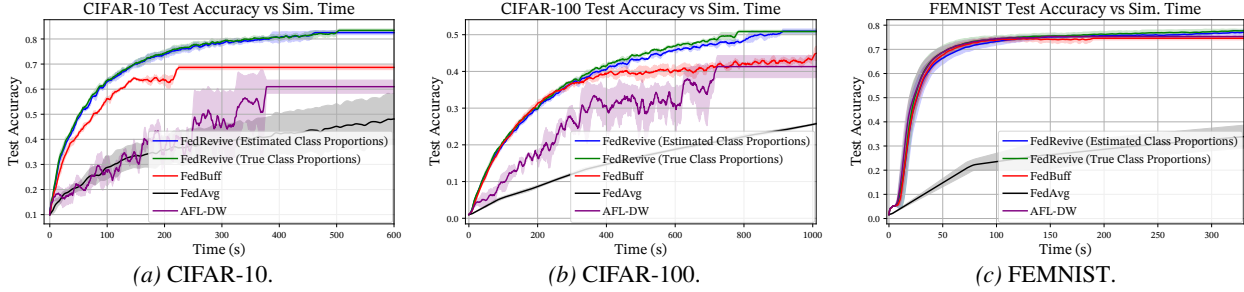


Figure 5. **FedRevive with estimated client label proportions.** Replacing ground-truth client label proportions with our probing-based proxies yields similar training dynamics and final performance across datasets.

C. FLOPs Analysis and Server Overhead Discussion

We quantify the additional computation introduced by FedRevive on the server by reporting FLOPs per processed sample for the dominant components of the pipeline: (i) client local training, (ii) server generator training and pseudo-sample synthesis, and (iii) server-side multi-teacher distillation. Table 3 compares these costs under our default hyperparameters.

Table 3. **Compute overhead breakdown (FLOPs) per sample for CIFAR-10 experiments.** FLOPs (G) for dominant components. c denotes the teacher buffer size.

[†]Rows report total compute except the last row, which reports effective blocking compute with concurrent implementation (total FLOPs unchanged).

Component	FLOPs (G) per iter [†]	Total across iters
Client local training (25 iters)	1.65	41.25
Generator train & synth. (at every T_{gen} rounds, amortized)	$0.14 + 0.11 c$	$0.28 + 0.22 c$
Distillation (sequential implementation, 10 iters)	$1.65 + 0.55 c$	$16.5 + 5.5 c$
Distillation (effective cost with concurrent implementation)	2.2	22

First, generator training and synthesis is performed for only $K_{synth} = 2$ iterations and only once every $T_{gen} = 10$ server updates, so its average cost is amortized by a factor of $T_{gen} = 10$ (second row block in Table 3). Second, distillation is run for $K_{KD}=10$ iterations, and its cost decomposes into student updates plus teacher forward passes. Since the server maintains a buffer of teachers, forward passes for all buffered teachers except the most recent arrival can be executed asynchronously while waiting for the next client upload; thus, the effective blocking compute can be close to the student-update cost (last row in Table 3).

Third, server computation does not need to add an extra wall-clock delay in an asynchronous system. Concretely, upon receiving a client update, the server can immediately dispatch the next local-training request using the current global state, and then perform synthesis, distillation, and hybrid aggregation in parallel. This re-ordering decouples client progress from server-side computation and primarily introduces only a small additional staleness relative to the already-present asynchrony.

Fourth, moderate server-side overhead is typically less critical than client-side computation and straggling, since modern servers are substantially more compute-capable than edge devices (Bonawitz et al., 2019). Moreover, in many practical FL deployments, especially wireless settings, communication latency can dominate end-to-end runtime (McMahan et al., 2017; Zhu et al., 2021a), so additional server compute often has limited impact on overall wall-clock training time.

Finally, we did not tune $K_{synth}, K_{KD}, T_{gen}$ to minimize FLOPs, since our focus is better convergence performance. In deployments where server budget is tighter, these hyperparameters can be reduced and periodic synthesis can be made more aggressive, further lowering amortized overhead.

D. Details on Time Simulation in Experiments

Delay simulation model. Our simulator assigns each client i three independent delay generators: local computation delay d_i^{train} (local training), downlink delay d_i^{down} (model download), and uplink delay d_i^{up} (update upload). A client’s realized end-to-end round-trip time is the sum of these components, and the staleness τ is induced by how many server updates occur while an update is in transit and being computed. Since the servers are generally equipped with much faster

hardware compared to client computation and communication delays, we model server-side operation time as non-blocking or overlapped (validated by measured runtimes) in our simulation, discussed in detail next. To model persistent heterogeneity, we first randomly sample a *client-specific mean* for each delay component, and keep it fixed for that client throughout training. The instantaneous delay values then vary around this mean according to the chosen distribution. The three components are sampled independently per client, so a client may be slow in computation but fast in communication, or vice versa.

Server-side runtime. We benchmark the wall-clock cost of the main computation blocks in our CIFAR-10 setup with batch size 32 under three representative configurations. On a 16-core CPU, a single client local-training run takes 4.874 s in total. Even when clients are equipped with a Tesla T4, local training still takes 0.657 s per run. In contrast, when the server is equipped with a modern accelerator (H100), the amortized synthesis runtime is 0.038 s per server update (with one generator update every 10 rounds), while distillation takes 0.110 s with a sequential implementation and 0.0569 s with an efficient non-blocking implementation. Furthermore, communication is typically the dominant bottleneck in cross-device FL (Lai et al., 2021; Zhu et al., 2021a). Therefore, we model comparatively small server-side operation time as non-blocking or overlapped in our simulation. Moreover, the server-side pipeline can be arranged to avoid introducing any additional wall-clock delay. The server can dispatch the next local-training request immediately upon receiving an update and run synthesis, distillation, and hybrid aggregation asynchronously afterward, which hides most server compute behind client-side latency at the cost of only a small additional staleness.

Mixture over client speeds. For each delay component, the client-specific mean is drawn from a discrete mixture distribution specified by a set of pairs $\{(p_k, \mu_k)\}_k$, where $\sum_k p_k = 1$. Concretely, with probability p_k the client is assigned mean delay μ_k for that component. This mixture produces multiple “speed tiers” and yields a long-tailed staleness distribution when combined with asynchronous execution.

Delay distributions and parameters. In our default configuration, the three delay components use different distributions: (i) *Local training delay* is exponential with a client-specific mean drawn from $\{(0.25, 1.0), (0.5, 1.3), (0.25, 1.6)\}$. (ii) *Download delay* is constant value 0.1 for all clients. (iii) *Upload delay* is uniform around a client-specific mean drawn from $\{(0.5, 0.15), (0.5, 0.25)\}$, using a half-width of 0.02 (i.e., sampled from $[\max(0, \mu - 0.02), \mu + 0.02]$). All delay quantities are in the simulator’s time units, and the above settings are used for all main experiments unless stated otherwise.

We plot the distribution of update staleness in server rounds from a sample experiment for a fully asynchronous algorithm in Figure 6. It is shown in the figure that the staleness distribution is long-tailed due to slow clients. The figure further validates the simulation’s alignment with real practice, matching the staleness distribution observed in real-world experiments with millions of clients (Nguyen et al., 2022).

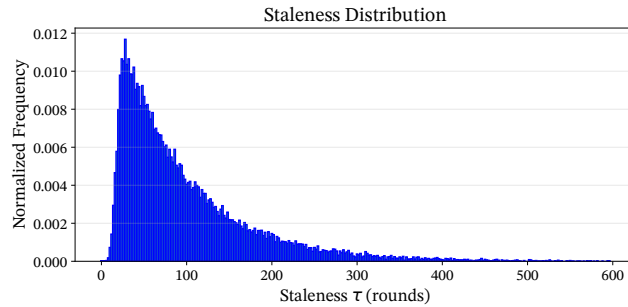


Figure 6. Distribution of update staleness across server rounds for a fully asynchronous setup. The distribution aligns with real-world AFL systems reported in Nguyen et al. (2022).

D.1. Modified Delay Schedule and Shifted Staleness Distribution

In the experiment for robustness to change in delay scheme in Section 3.2, to evaluate robustness to system changes, we modify the parameters of the computation and communication delay distributions in the simulator, which yields a different induced staleness distribution (Figure 7) than the default setting used throughout the main experiments (Figure 6). In this robustness evaluation, we keep exactly the same hyperparameters for every method as tuned under the default delay scheme,

and only change the delay sampling mechanism.

Modified delay parameters. Under the modified delay schedule, we use: (i) an exponential local training delay whose client-specific mean set at 0.1, (ii) a constant download delay with mean 0.02 for all clients (iii) a uniform upload delay with client-specific mean sampled from $\{(0.5, 0.05), (0.5, 0.10)\}$ and half-width 0.01 (i.e., sampled from $[\max(0, \mu - 0.01), \mu + 0.01]$). All other aspects of the simulator remain unchanged.

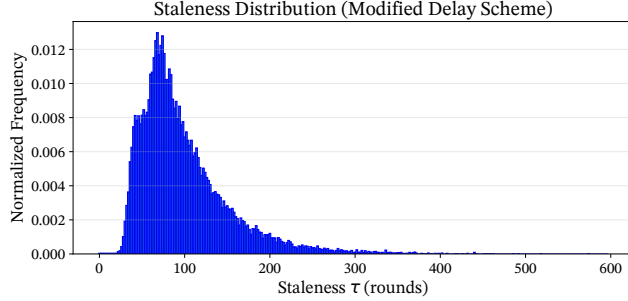


Figure 7. Staleness distribution induced by the modified delay schedule used in the experiment for robustness to change in delay scheme in Section 3.2. For reference, the default distribution is shown in Figure 6.

E. Results with a Milder Heterogeneity Level

We provide additional experimental results under different levels of data heterogeneity. For the CIFAR-10, CIFAR-100, and 20NewsGroups datasets, we show the test accuracy curves when client data is distributed with milder non-IID partition ($\alpha = 1$). See Figure 8 for the results. Note that the FEMNIST dataset is naturally partitioned by real users and thus does not allow controlling its heterogeneity. Hence, it is excluded from this analysis. All hyperparameters except data heterogeneity are kept the same as those of main experiments.

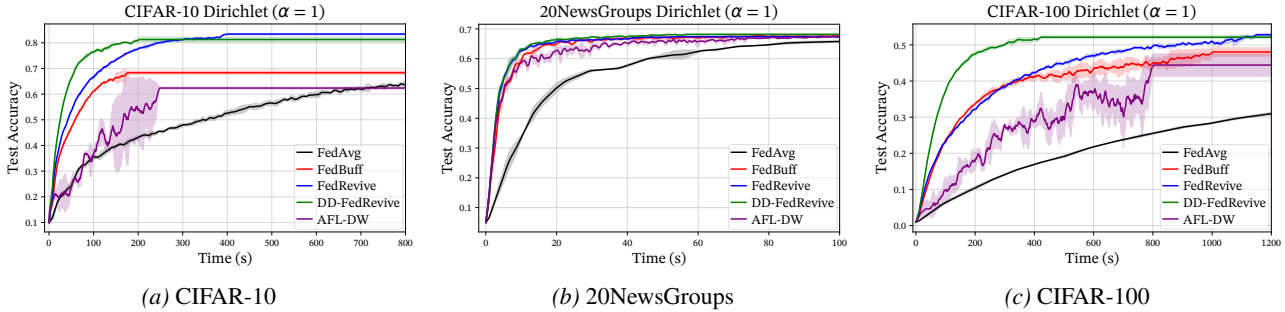


Figure 8. Test accuracy over simulated time under milder heterogeneity ($\alpha = 1$). FedRevive converges faster than FedBuff and achieves higher final accuracy across datasets.

F. Raw Training Curves without Running Average Processing

As described in the main text, asynchronous algorithms often display fluctuations in performance due to delayed updates and highly heterogeneous model aggregation. To provide a clearer comparison, the main figures report the moving-averaged test accuracy over time. Here, we present the original unprocessed curves showing the raw test accuracy trajectories. Figure 9 illustrates these curves.

G. Update Ablations for DFKD and the Role of $\beta(\tau)$

This section complements experiments on the update contributions in DFKD in Section 3.2. We ablate the contribution of update components in Eq. 3 on CIFAR-10 by measuring their effect separately at each server round, applying either (i) only

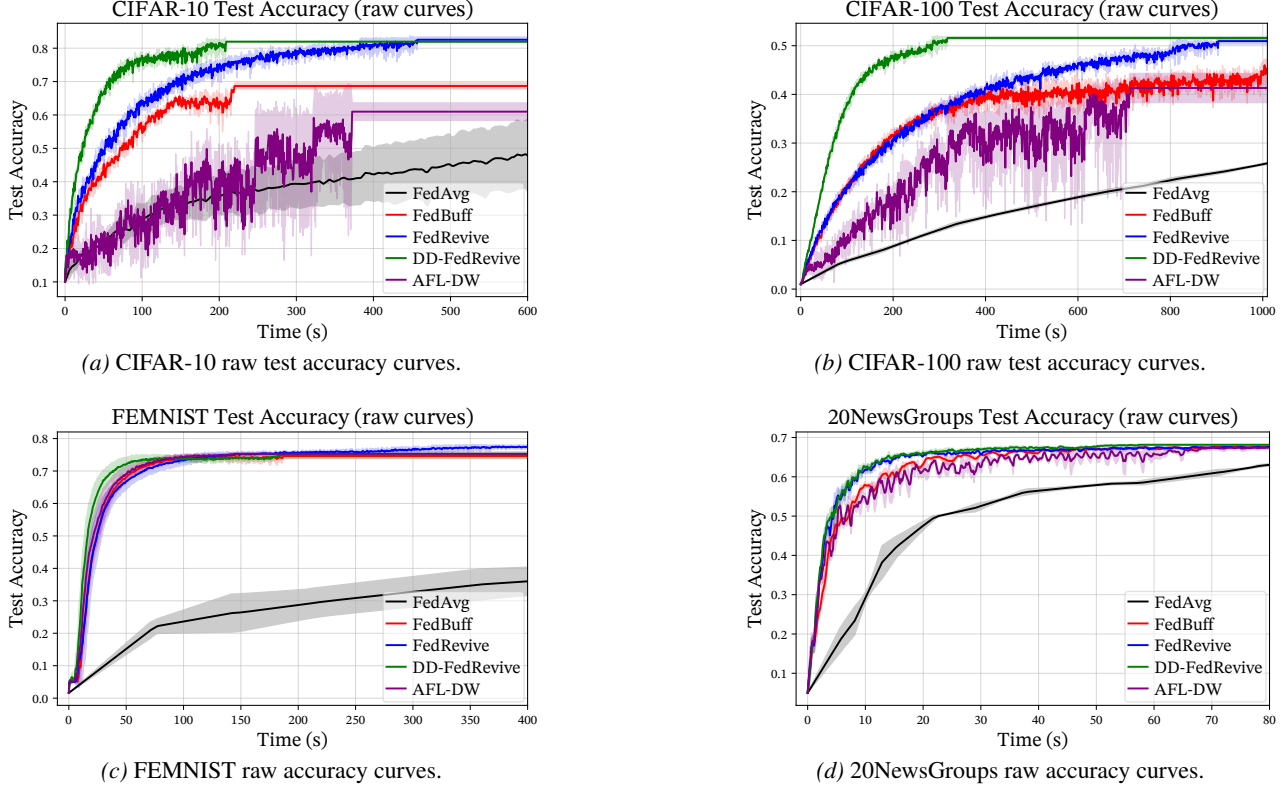


Figure 9. Raw accuracy curves across datasets ($\alpha = 0.5$).

the stale client update $\Delta_i^{(t-\tau_i^t)}$, (ii) only the KD-revived update Δ_i^{KD} from $\text{KD-Revive}(\cdot)$, or (iii) the combined update in Eq. 3. We evaluate three mixing regimes: (a) the adaptive $\beta(\tau)$ schedule used in the main paper, (b) a fixed $\beta(\tau) = 0.75$, and (c) a fixed $\beta(\tau) = 1$.

Figure 10a shows that under adaptive $\beta(\tau)$ the combined update yields the best overall performance, and the KD-revived component is crucial for rapid gains. However, KD alone does not replace the stale client update: retaining the client update is necessary for sustained learning across rounds. Figures 10b and 10c further indicate that fixing β to a high value such as 0.75 or 1 leads to lower long-run accuracy compared to the adaptive schedule due to lacking the contribution of original client updates, underscoring the importance of staleness-adaptive mixing.

H. Server Memory Footprint of FedRevive

Global-model storage. FedRevive does not require additional server memory beyond what is already standard in asynchronous FL, aside from the (constant-sized) teacher buffer. The server maintains the current global model $\mathbf{x}^{(t)}$ as usual. When an upload $\tilde{\mathbf{x}}_i^{(t-\tau_i^t)}$ arrives, forming the corresponding difference update $\Delta_i = \tilde{\mathbf{x}}_i - \mathbf{x}$ may appear to require retaining an extra copy of \mathbf{x} . However, this does not introduce a new storage requirement: conventional FL must also keep both the pre-training model and the post-training model either at the server or at the client in the system in order to form Δ_i (clients typically compute $\tilde{\mathbf{x}}_i - \mathbf{x}$ locally). FedRevive simply computes the same quantity on the server.

Implementation without explicit updates. In addition, implementations can avoid materializing Δ_i entirely by updating the global parameters directly through interpolation in parameter space. For example, a standard aggregation step with learning rate η_s can be written as

$$\mathbf{x}^{(t+1)} = (1 - \eta_s) \mathbf{x}^{(t)} + \eta_s \tilde{\mathbf{x}}_i^{(t-\tau_i^t)},$$

which can be evaluated in-place without storing an explicit update vector. Therefore, FedRevive has the same model-storage footprint as vanilla asynchronous FL, except the constant-sized teacher buffer.

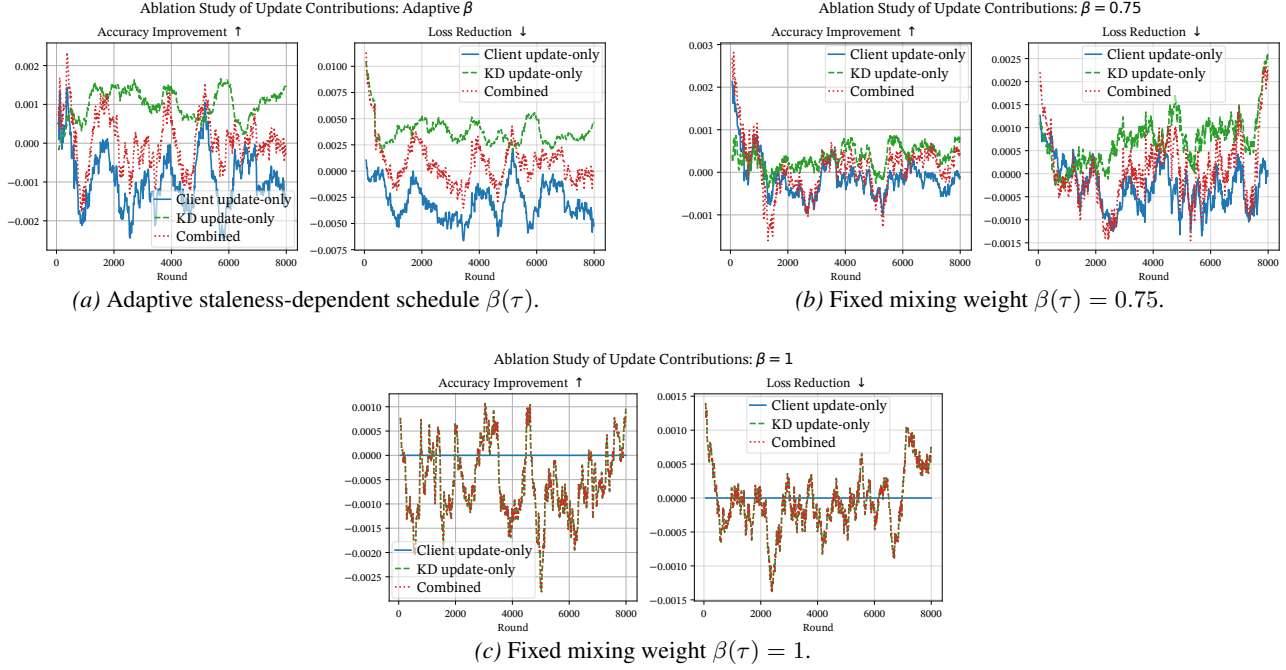


Figure 10. CIFAR-10 Update-component ablation under adaptive and fixed mixing-weight schedules.

I. Experimental Details and Hyperparameters

Data partitioning and seeds. We simulate 1000 clients. For all tasks, each client holds 350 training examples, and client datasets are sampled using a non-iid Dirichlet partition. We use 15% of the full dataset for validation, 15% for test. All results are averaged over three random seeds.

Client optimization. Clients train with Adam ($\beta_1 = 0.9$), local batch size 32, and 25 local iterations per client update. In asynchronous runs, 100 clients are active concurrently out of 1000 total clients. In synchronous runs, 100 clients join a single round.

Learning rates. We tune the client learning rate η_c and server learning rate η_s per method and dataset. Table 4 reports the final choices. For AFL-DW, we use the same learning rates as FedRevive. For FedBuff, we set the buffer size to 2 (CIFAR-10), 3 (CIFAR-100), 1 (FEMNIST), and 3 (20NewsGroups).

KD augmentation settings. Both KD-based variants use a teacher buffer of size $c = 8$ and a KD batch size of 32.

DD-FedRevive hyperparameters. We run 10 distillation steps per server update, and fix the mixing coefficient to $\beta = 0.5$. Table 5 reports the student learning rate used inside KD and the distillation temperature.

FedRevive hyperparameters. We use synthesis batch size 64 and KD batch size 32. Per server update, we perform 10 KD steps and update the generator for 2 steps before meta learning step once at every 10 server updates. The KD temperature is fixed to $T = 1$. For the synthesis loss in Eq. 4, we fix the adversarial and target alignment weights to $\alpha_{adv} = 0.1$ and $\alpha_{target} = 1.0$, and set the feature matching weight $\alpha_{feature}$ per dataset (Table 6). For the aggregation mixing, FedRevive uses the adaptive schedule described in the main text.

Feature statistics used in $\mathcal{L}_{feature}$. The feature loss in Eq. 4 matches architecture-specific intermediate statistics via $\phi(\cdot)$. For the vision backbones (ResNet-18 on CIFAR-10/CIFAR-100 and the CNN on FEMNIST), we follow standard DFKD practice and use BatchNorm statistics. For the transformer model (20NewsGroups with T5-small), we use hidden-states at the position of classification head (first token).

Table 4. Client and server learning rates used in each experiment.

Dataset	Method	η_c	η_s	FedBuff buffer size
CIFAR-10	FedAvg	0.0003	1.4	–
	FedBuff	0.0003	0.05	2
	AFL-DW	0.0003	0.10	–
	DD-FedRevive	0.0003	0.20	–
	FedRevive	0.0003	0.10	–
CIFAR-100	FedAvg	0.0003	1.4	–
	FedBuff	0.0003	0.10	3
	AFL-DW	0.0003	0.10	–
	DD-FedRevive	0.0001	0.30	–
	FedRevive	0.0003	0.10	–
FEMNIST	FedAvg	0.001	1.4	–
	FedBuff	0.001	0.025	1
	AFL-DW	0.001	0.05	–
	DD-FedRevive	0.001	0.10	–
	FedRevive	0.001	0.05	–
20NewsGroups	FedAvg	0.003	1.0	–
	FedBuff	0.001	0.1	3
	AFL-DW	0.001	0.1	–
	DD-FedRevive	0.001	0.1	–
	FedRevive	0.001	0.1	–

 Table 5. Hyperparameters for DD-FedRevive. Shared: 10 distillation steps per server update, distillation batch size 32, teacher buffer size $c = 8$, and $\beta = 0.5$ (constant for DD-FedRevive).

Dataset	KD learning rate	Distillation temperature
CIFAR-10	0.0003	2.0
CIFAR-100	0.0001	2.0
FEMNIST	0.0003	2.0
20NewsGroups	0.0001	2.0

I.1. β Scheduling Families

We consider several candidate monotone scheduling families for β , which determines how quickly FedRevive shifts from parameter-space aggregation to KD-dominated aggregation as staleness increases. Figure 11 visualizes the families we considered. Unless stated otherwise, we use the $1 - \cos$ schedule in all experiments.

Table 6. Dataset-specific DFKD hyperparameters for FedRevive. Shared: synthesis batch size 64, KD batch size 32, teacher buffer size 8, KD temperature $T = 1$, 2 generator steps every 10 server updates, and 10 KD steps per server update. Learning rates (LR) are presented in the table.

Dataset	KD LR	Generator LR	Latent noise LR	α_{feature}
CIFAR-10	1e-4	0.003	0.001	0.003
CIFAR-100	3e-5	0.003	0.001	0.0003
FEMNIST	1e-4	0.01	0.003	0.3
20NewsGroups	3e-4	0.01	0.1	0.0001

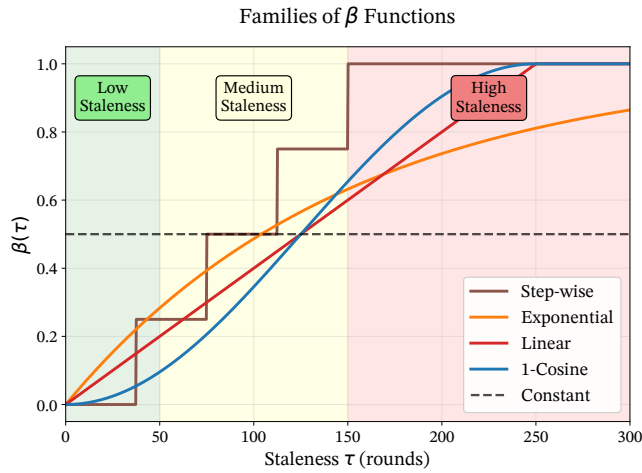


Figure 11. Different candidate β scheduling functions controlling the mix between parameter aggregation and DFKD updates. 1 – cosine schedule is chosen, as it empirically shows the best performance on the CIFAR-10 task.